DESY 98-076
June 1998

ISSN 0418-9833

Di-jet Event Rates in Deep-Inelastic Scattering at HERA

H1 Collaboration

hep-ex/9806029 v2 29 Jun 1998

Abstract

Di-jet event rates have been measured for deep-inelastic scattering in the kinematic domain $5 \lesssim Q^2 \lesssim 100$ GeV^2 and $10^{-4} \lesssim x_{Bj} \lesssim 10^{-2}$, and for jet transverse momenta squared $p_t^2 \gtrsim Q^2$. The analysis is based on data collected with the H1 detector at HERA in 1994 corresponding to an integrated luminosity of about 2 pb^{-1}. Jets are defined using a cone algorithm in the photon-proton centre of mass system requiring jet transverse momenta of at least 5 GeV. The di-jet event rates are shown as a function of Q^2 and x_{Bj}. Leading order models of point-like interacting photons fail to describe the data. Models which add resolved interacting photons or which implement the colour dipole model give a good description of the di-jet event rate. This is also the case for next-to-leading order calculations including contributions from direct and resolved photons.

Submitted to the European Physical Journal

C. Adloff[35], S. Aid[13], M. Anderson[23], V. Andreev[26], B. Andrieu[29], V. Arkadov[36], C. Arndt[11], I. Ayyaz[30], A. Babaev[25], J. Bähr[36], J. Bán[18], P. Baranov[26], E. Barrelet[30], R. Barschke[11], W. Bartel[11], U. Bassler[30], M. Beck[14], H.-J. Behrend[11], C. Beier[16], A. Belousov[26], Ch. Berger[1], G. Bernardi[30], G. Bertrand-Coremans[4], R. Beyer[11], P. Biddulph[23], J.C. Bizot[28], K. Borras[8], V. Boudry[29], S. Bourov[25], A. Braemer[15], W. Braunschweig[1], V. Brisson[28], D.P. Brown[23], W. Brückner[14], P. Bruel[29], D. Bruncko[18], C. Brune[16], J. Bürger[11], F.W. Büsser[13], A. Buniatian[4], S. Burke[19], G. Buschhorn[27], D. Calvet[24], A.J. Campbell[11], T. Carli[27], M. Charlet[11], D. Clarke[5], B. Clerbaux[4], S. Cocks[20], J.G. Contreras[8], C. Cormack[20], J.A. Coughlan[5], M.-C. Cousinou[24], B.E. Cox[23], G. Cozzika[9], J. Cvach[31], J.B. Dainton[20], W.D. Dau[17], K. Daum[40], M. David[9], M. Davidsson[22], A. De Roeck[11], E.A. De Wolf[4], B. Delcourt[28], M. Dirkmann[8], P. Dixon[19], W. Dlugosz[7], K.T. Donovan[21], J.D. Dowell[3], A. Droutskoi[25], J. Ebert[35], T.R. Ebert[20], G. Eckerlin[11], V. Efremenko[25], S. Egli[38], R. Eichler[37], F. Eisele[15], E. Eisenhandler[21], E. Elsen[11], M. Erdmann[15], A.B. Fahr[13], L. Favart[28], A. Fedotov[25], R. Felst[11], J. Feltesse[9], J. Ferencei[18], F. Ferrarotto[33], K. Flamm[11], M. Fleischer[8], M. Flieser[27], G. Flügge[2], A. Fomenko[26], J. Formánek[32], J.M. Foster[23], G. Franke[11], E. Gabathuler[20], K. Gabathuler[34], F. Gaede[27], J. Garvey[3], J. Gayler[11], M. Gebauer[36], R. Gerhards[11], A. Glazov[36], L. Goerlich[6], N. Gogitidze[26], M. Goldberg[30], I. Gorelov[25], C. Grab[37], H. Grässler[2], T. Greenshaw[20], R.K. Griffiths[21], G. Grindhammer[27], A. Gruber[27], C. Gruber[17], T. Hadig[1], D. Haidt[11], L. Hajduk[6], T. Haller[14], M. Hampel[1], W.J. Haynes[5], B. Heinemann[11], G. Heinzelmann[13], R.C.W. Henderson[19], S. Hengstmann[38], H. Henschel[36], R. Heremans[4], I. Herynek[31], K. Hewitt[3], K.H. Hiller[36], C.D. Hilton[23], J. Hladký[31], M. Höppner[8], D. Hoffmann[11], T. Holtom[20], R. Horisberger[34], V.L. Hudgson[3], M. Hütte[8], M. Ibbotson[23], Ç. İşsever[8], H. Itterbeck[1], M. Jacquet[28], M. Jaffre[28], J. Janoth[16], D.M. Jansen[14], L. Jönsson[22], D.P. Johnson[4], H. Jung[22], P.I.P. Kalmus[21], M. Kander[11], D. Kant[21], M. Karlsson[22], U. Kathage[17], J. Katzy[15], H.H. Kaufmann[36], O. Kaufmann[15], M. Kausch[11], S. Kazarian[11], I.R. Kenyon[3], S. Kermiche[24], C. Keuker[1], C. Kiesling[27], M. Klein[36], C. Kleinwort[11], G. Knies[11], J.H. Köhne[27], H. Kolanoski[39], S.D. Kolya[23], V. Korbel[11], P. Kostka[36], S.K. Kotelnikov[26], T. Krämerkämper[8], M.W. Krasny[6,30], H. Krehbiel[11], D. Krücker[27], A. Küpper[35], H. Küster[22], M. Kuhlen[27], T. Kurča[36], B. Laforge[9], R. Lahmann[11], M.P.J. Landon[21], W. Lange[36], U. Langenegger[37], A. Lebedev[26], F. Lehner[11], V. Lemaitre[11], S. Levonian[29], M. Lindstroem[22], J. Lipinski[11], B. List[11], G. Lobo[28], G.C. Lopez[12], V. Lubimov[25], D. Lüke[8,11], L. Lytkin[14], N. Magnussen[35], H. Mahlke-Krüger[11], E. Malinovski[26], R. Maraček[18], P. Marage[4], J. Marks[15], R. Marshall[23], J. Martens[35], G. Martin[13], R. Martin[20], H.-U. Martyn[1], J. Martyniak[6], S.J. Maxfield[20], S.J. McMahon[20], A. Mehta[5], K. Meier[16], P. Merkel[11], F. Metlica[14], A. Meyer[13], A. Meyer[11], H. Meyer[35], J. Meyer[11], P.-O. Meyer[2], A. Migliori[29], S. Mikocki[6], D. Milstead[20], J. Moeck[27], F. Moreau[29], J.V. Morris[5], E. Mroczko[6], D. Müller[38], K. Müller[11], P. Murín[18], V. Nagovizin[25], R. Nahnhauer[36], B. Naroska[13], Th. Naumann[36], I. Négri[24], P.R. Newman[3], D. Newton[19], H.K. Nguyen[30], T.C. Nicholls[3], F. Niebergall[13], C. Niebuhr[11], Ch. Niedzballa[1], H. Niggli[37], G. Nowak[6], T. Nunnemann[14], H. Oberlack[27], J.E. Olsson[11], D. Ozerov[25], P. Palmen[2], E. Panaro[11], A. Panitch[4], C. Pascaud[28], S. Passaggio[37], G.D. Patel[20], H. Pawletta[2], E. Peppel[36], E. Perez[9], J.P. Phillips[20], A. Pieuchot[24], D. Pitzl[37], R. Pöschl[8], G. Pope[7], B. Povh[14], K. Rabbertz[1], P. Reimer[31], H. Rick[8], S. Riess[13], E. Rizvi[11],

P. Robmann[38], R. Roosen[4], K. Rosenbauer[1], A. Rostovtsev[30], F. Rouse[7], C. Royon[9], K. Rüter[27], S. Rusakov[26], K. Rybicki[6], D.P.C. Sankey[5], P. Schacht[27], J. Scheins[1], S. Schiek[11], S. Schleif[16], W. von Schlippe[21], D. Schmidt[35], G. Schmidt[11], L. Schoeffel[9], A. Schöning[11], V. Schröder[11], E. Schuhmann[27], H.-C. Schultz-Coulon[11], B. Schwab[15], F. Sefkow[38], A. Semenov[25], V. Shekelyan[11], I. Sheviakov[26], L.N. Shtarkov[26], G. Siegmon[17], U. Siewert[17], Y. Sirois[29], I.O. Skillicorn[10], T. Sloan[19], P. Smirnov[26], M. Smith[20], V. Solochenko[25], Y. Soloviev[26], A. Specka[29], J. Spiekermann[8], S. Spielman[29], H. Spitzer[13], F. Squinabol[28], P. Steffen[11], R. Steinberg[2], J. Steinhart[13], B. Stella[33], A. Stellberger[16], J. Stiewe[16], K. Stolze[36], U. Straumann[15], W. Struczinski[2], J.P. Sutton[3], M. Swart[16], S. Tapprogge[16], M. Taševský[32], V. Tchernyshov[25], S. Tchetchelnitski[25], J. Theissen[2], G. Thompson[21], P.D. Thompson[3], N. Tobien[11], R. Todenhagen[14], P. Truöl[38], J. Zálešák[32], G. Tsipolitis[37], J. Turnau[6], E. Tzamariudaki[11], P. Uelkes[2], A. Usik[26], S. Valkár[32], A. Valkárová[32], C. Vallée[24], P. Van Esch[4], P. Van Mechelen[4], D. Vandenplas[29], Y. Vazdik[26], P. Verrecchia[9], G. Villet[9], K. Wacker[8], A. Wagener[2], M. Wagener[34], R. Wallny[15], T. Walter[38], B. Waugh[23], G. Weber[13], M. Weber[16], D. Wegener[8], A. Wegner[27], T. Wengler[15], M. Werner[15], L.R. West[3], S. Wiesand[35], T. Wilksen[11], S. Willard[7], M. Winde[36], G.-G. Winter[11], C. Wittek[13], M. Wobisch[2], H. Wollatz[11], E. Wünsch[11], J. Žáček[32], D. Zarbock[12], Z. Zhang[28], A. Zhokin[25], P. Zini[30], F. Zomer[28], J. Zsembery[9], and M. zurNedden[38],

[1] I. Physikalisches Institut der RWTH, Aachen, Germany[a]
[2] III. Physikalisches Institut der RWTH, Aachen, Germany[a]
[3] School of Physics and Space Research, University of Birmingham, Birmingham, UK[b]
[4] Inter-University Institute for High Energies ULB-VUB, Brussels; Universitaire Instelling Antwerpen, Wilrijk; Belgium[c]
[5] Rutherford Appleton Laboratory, Chilton, Didcot, UK[b]
[6] Institute for Nuclear Physics, Cracow, Poland[d]
[7] Physics Department and IIRPA, University of California, Davis, California, USA[e]
[8] Institut für Physik, Universität Dortmund, Dortmund, Germany[a]
[9] DSM/DAPNIA, CEA/Saclay, Gif-sur-Yvette, France
[10] Department of Physics and Astronomy, University of Glasgow, Glasgow, UK[b]
[11] DESY, Hamburg, Germany[a]
[12] I. Institut für Experimentalphysik, Universität Hamburg, Hamburg, Germany[a]
[13] II. Institut für Experimentalphysik, Universität Hamburg, Hamburg, Germany[a]
[14] Max-Planck-Institut für Kernphysik, Heidelberg, Germany[a]
[15] Physikalisches Institut, Universität Heidelberg, Heidelberg, Germany[a]
[16] Institut für Hochenergiephysik, Universität Heidelberg, Heidelberg, Germany[a]
[17] Institut für Reine und Angewandte Kernphysik, Universität Kiel, Kiel, Germany[a]
[18] Institute of Experimental Physics, Slovak Academy of Sciences, Košice, Slovak Republic[f,j]
[19] School of Physics and Chemistry, University of Lancaster, Lancaster, UK[b]
[20] Department of Physics, University of Liverpool, Liverpool, UK[b]
[21] Queen Mary and Westfield College, London, UK[b]
[22] Physics Department, University of Lund, Lund, Sweden[g]
[23] Physics Department, University of Manchester, Manchester, UK[b]

[24] CPPM, Université d'Aix-Marseille II, IN2P3-CNRS, Marseille, France
[25] Institute for Theoretical and Experimental Physics, Moscow, Russia
[26] Lebedev Physical Institute, Moscow, Russia[f,k]
[27] Max-Planck-Institut für Physik, München, Germany[a]
[28] LAL, Université de Paris-Sud, IN2P3-CNRS, Orsay, France
[29] LPNHE, Ecole Polytechnique, IN2P3-CNRS, Palaiseau, France
[30] LPNHE, Universités Paris VI and VII, IN2P3-CNRS, Paris, France
[31] Institute of Physics, Czech Academy of Sciences of the Czech Republic, Praha, Czech Republic[f,h]
[32] Nuclear Center, Charles University, Praha, Czech Republic[f,h]
[33] INFN Roma 1 and Dipartimento di Fisica, Università Roma 3, Roma, Italy
[34] Paul Scherrer Institut, Villigen, Switzerland
[35] Fachbereich Physik, Bergische Universität Gesamthochschule Wuppertal, Wuppertal, Germany[a]
[36] DESY, Institut für Hochenergiephysik, Zeuthen, Germany[a]
[37] Institut für Teilchenphysik, ETH, Zürich, Switzerland[i]
[38] Physik-Institut der Universität Zürich, Zürich, Switzerland[i]
[39] Institut für Physik, Humboldt-Universität, Berlin, Germany[a]
[40] Rechenzentrum, Bergische Universität Gesamthochschule Wuppertal, Wuppertal, Germany[a]

[a] Supported by the Bundesministerium für Bildung, Wissenschaft, Forschung und Technologie, FRG, under contract numbers 7AC17P, 7AC47P, 7DO55P, 7HH17I, 7HH27P, 7HD17P, 7HD27P, 7KI17I, 6MP17I and 7WT87P
[b] Supported by the UK Particle Physics and Astronomy Research Council, and formerly by the UK Science and Engineering Research Council
[c] Supported by FNRS-NFWO, IISN-IIKW
[d] Partially supported by the Polish State Committee for Scientific Research, grant no. 115/E-343/SPUB/P03/002/97 and grant no. 2P03B 055 13
[e] Supported in part by US DOE grant DE F603 91ER40674
[f] Supported by the Deutsche Forschungsgemeinschaft
[g] Supported by the Swedish Natural Science Research Council
[h] Supported by GA ČR grant no. 202/96/0214, GA AV ČR grant no. A1010619 and GA UK grant no. 177
[i] Supported by the Swiss National Science Foundation
[j] Supported by VEGA SR grant no. 2/1325/96
[k] Supported by Russian Foundation for Basic Researches grant no. 96-02-00019

1 Introduction

The study of jets in deep-inelastic lepton-proton scattering (DIS) provides a testing ground for perturbative QCD. Partons emerging from the scattering process manifest themselves as jets of collimated hadrons which are observable in the experiment.

In the naive quark parton model, the virtual photon is absorbed by a single quark (antiquark) of the proton resulting in one jet from the struck quark and one from the proton remnant. Both jets have no transverse momentum in the photon-proton centre of mass frame (cms), when neglecting the intrinsic motion of the partons inside the proton. To first order in α_s, the leading order (LO) for di-jet production, two jets with balanced transverse momenta in the photon-proton cms are produced in the hard scattering process, in addition to the proton remnant jet. The hard scattering can either be the quark initiated QCD-Compton (QCDC) or the gluon initiated photon-gluon fusion (BGF) process.

In this analysis we present a measurement of the fraction R_2 of di-jet events in all DIS events, referred to as the di-jet rate. It is presented as a function of the Bjorken scaling variable x_{Bj}, integrated over the virtuality of the exchanged photon Q^2, and of Q^2, integrated over x_{Bj}. Jets are defined using a cone algorithm in the photon-proton cms requiring jet transverse momenta of at least 5 GeV. The measured jet rates are corrected for detector effects.

Previous measurements of jet rates at HERA [1] used the JADE jet algorithm at photon virtualities Q^2 large compared to the squared jet transverse momenta p_t^2. The present analysis probes a region of jet phase space characterized by jet transverse momenta squared of similar size or larger than the photon virtuality, $p_t^2/Q^2 \gtrsim 1$. It has significantly better precision and has its emphasis on higher Q^2 compared to a previous study of single inclusive jet production [2]. There the data were found to be in good agreement with LO QCD models which included a resolved partonic structure of the virtual photon that evolves with Q^2.

In this study we investigate whether the di-jet rate can be described by LO QCD models with just point-like (direct) interactions of the virtual photon and with models with additional contributions from resolved photons, which may be considered as an effective description of higher order QCD effects. We also consider the colour dipole model. Finally our measurements are compared to next-to-leading order (NLO) QCD calculations which include either only direct or direct and resolved virtual photons.

The measurement was performed using data taken in 1994 with the H1 detector at the HERA storage ring, where 27.5 GeV positrons were collided with 820 GeV protons.

2 The H1 Detector

A detailed description of the H1 apparatus is given elsewhere [3]. The parts of the detector which are essential for this measurement are the liquid argon (LAr) calorimeter [4], the backward lead-scintillator calorimeter (BEMC) [5], and the tracking chamber system.

The energy of the scattered positron is measured in the BEMC which covers the range

in polar angle[1], θ, from 151° to 176°. It consists of stacks of lead and scintillator plates with a total of 21.7 radiation lengths. The BEMC is laterally segmented into square modules of $16 \times 16\,\mathrm{cm}^2$, with smaller modules at the inner and outer radii. The scintillation light is read out with photodiodes via wave length shifters along two opposite sides of each module. The absolute energy scale was determined to a precision of 1% [6]. The energy resolution is given by $\sigma_E/E = 39\%/E \oplus 10\%/\sqrt{E} \oplus 1.7\%$ (E in GeV) [5].

A cluster energy deposition exceeding a threshold of $\approx 7\,\mathrm{GeV}$ in the BEMC was the primary trigger condition for events used in this analysis.

The position of the scattered positron is measured with the backward proportional chamber (BPC) located in front of the BEMC covering the angular range $155° < \theta < 174.5°$. The BPC consists of four layers of wires strung vertically, horizontally, and at $\pm 45°$. The position resolution is $\sigma_{x,y} = 1.5\,\mathrm{mm}$.

Hadronic energy is detected in the highly segmented (≈ 45000 channels) LAr calorimeter which extends from $4° < \theta < 154°$. The depth of the LAr calorimeter varies between 4.5 and 8 hadronic interaction lengths in the region $4° < \theta < 128°$. The uncertainty of the energy scale for hadrons is 4%. The hadronic energy resolution is $\sigma_E/E = 50\%/\sqrt{E} \oplus 2\%$ (E in GeV), as measured with test beams [7].

Charged tracks in the central region ($25° < \theta < 155°$) are measured with the central drift chamber system. Two jet chambers with wires in the z-direction allow measurements of track positions in the r-ϕ-plane to a precision of $\sigma_{r\phi} = 170\,\mu\mathrm{m}$. The z coordinate is measured to a precision of $\sigma_z = 320\,\mu\mathrm{m}$ using drift chambers with wires forming approximate circles around the beam. The momentum resolution is $\sigma_{p_t}/p_t^2 < 1\%\ \mathrm{GeV}^{-1}$.

The forward tracking detector covers $7° < \theta < 25°$ and consists of drift chambers with alternating planes of parallel wires and others with wires in the radial direction. It allows the measurement of track segments to a precision of $\sigma_{x,y} \leq 200\,\mu\mathrm{m}$.

Two electromagnetic calorimeters located downstream in the positron beam direction measure positrons and photons from the bremsstrahlung process $ep \to ep\gamma$ for the purpose of luminosity determination.

3 Data Selection

The data sample used for the present analysis corresponds to an integrated luminosity of 1.97 pb^{-1} taken during the 1994 run period. The phase space region of DIS events considered in this analysis is defined as follows:

$$\begin{aligned} 156° < \quad & \theta_e & < 173° \\ & E' & > 11\,\mathrm{GeV} \\ & y & > 0.05 \end{aligned} \tag{1}$$

Here, θ_e is the polar angle of the scattered positron and E' is its energy. The variables x_{Bj}, Q^2 and y (the inelasticity variable) are all determined from the 4-vector of the scattered positron. This selection ensures that the scattered positron is well inside the acceptance region of the BEMC, that the trigger efficiency is high, that the kinematic variables

[1]The polar angle θ is defined with respect to the positive z-axis, the proton beam direction.

are well reconstructed, and that photoproduction background and radiative corrections are small. Photoproduction events, where the scattered positron is not detected in the backward direction, form a background if a particle from the hadronic final state entering the BEMC is misidentified as the scattered positron.

Additional cuts are applied for the identification of the scattered positron and to further suppress the influence of QED radiation and photoproduction background [6, 8]:

- The event must have a reconstructed vertex with a z position within ± 30 cm of the nominal position.
- The candidate positron shower is required to have a small lateral spread by applying the cut $r_{\rm clust} < 5$ cm, where $r_{\rm clust}$ is the energy-weighted mean transverse distance from the shower centre of gravity of each energy deposition sampled by the photodiodes.
- There must be a BPC signal within 5 cm of the straight line connecting the shower centre with the event vertex.
- The quantity $\sum_i (E_i - p_{z,i})$, where the sum is over all calorimeter energy depositions in the final state, is expected to be equal to twice the positron beam energy. An undetected positron in a photoproduction event or initial state photon radiation will decrease the value of this observable. For this analysis, $35 < \sum_i (E_i - p_{z,i}) < 70$ GeV is required.

4 Jet Reconstruction and Selection

Jets are reconstructed using clusters of energy [3] measured in the LAr calorimeter. Cluster energies are corrected for the difference in response to hadronic and electromagnetic energy deposition and for losses due to dead material and cracks. The cluster energy and the direction from the interaction point to the cluster centre are used to construct a massless four-vector.

The calorimetric energy measurement can be improved for low energy particles by using in addition to the energy the measured momentum of each charged particle track. To avoid double counting of energy each track was allowed to contribute at most 300 MeV. The value of 300 MeV was found to be optimal for reconstructing the transverse momenta of jets in simulated events [8].

Jets are defined in this analysis using a cone algorithm [9]. A cone is defined by a circular area of radius R in the $\eta^* - \phi^*$ plane, where η^* and ϕ^* are the pseudo-rapidity[2] and azimuthal angle in the photon-proton cms[3]. A jet candidate consists of all objects (clusters and tracks) whose massless four vectors fall inside a cone. The jet transverse momentum $p^*_{t,\rm jet}$ is calculated as the scalar sum of the transverse momenta p^*_t of the jet objects. The jet η^* and ϕ^* (jet direction) are calculated as the p^*_t-weighted averages of the η^* and ϕ^* of the objects. This way of calculating the jet parameters is usually called

[2] The pseudo-rapidity η^* is given by $-\ln\tan(\theta^*/2)$.

[3] Variables measured in the photon-proton cms are marked by a *. The positive z direction is defined to be along the incident proton direction.

the "p_t"-scheme [10]. An iterative procedure is used to find the jets of an event. Initially, every object in turn is used to define the cone centre of a candidate jet. The jet directions of the candidate jets[4] are then used as the cone centres for the next iteration. This is repeated until the resulting jet directions are identical to the cone centres. Then, also the midpoint in the $\eta^* - \phi^*$ plane of each pair of jets is considered as a candidate jet centre, and the procedure is repeated. Jets which have more than a fraction f of their $p^*_{t,\mathrm{jet}}$ contained in a higher transverse momentum jet are discarded. Finally, $p^*_{t,\mathrm{jet}}$ is required to exceed a minimum value $p^*_{t,\mathrm{min}}$.

In this analysis, the following parameters were chosen:

$$R = 1, \quad p^*_{t,\mathrm{min}} = 5\,\mathrm{GeV}, \quad \text{and } f = 0.75. \tag{2}$$

Exactly two jets per event fulfilling these criteria are demanded. In addition, the pseudo-rapidity difference $\Delta\eta^*$ of the two jets is required to be in the range

$$|\Delta\eta^*| < 2. \tag{3}$$

In leading order this cut is equivalent to requiring $|\cos\hat{\theta}| < 0.76$, where $\hat{\theta}$ is the polar angle between the emerging and incoming partons in the parton-parton or gamma-parton cms. It separates the jets from the proton remnant. The resolution in jet transverse momentum $\Delta p^*_t / p^*_t$ is approximately 20% at $p^*_t \sim 5$ GeV.

The number of di-jet events found is 4 957 while the total number of DIS events selected amounts to 112 806. To obtain the di-jet rate R_2, the number of di-jet events is divided by the total number of events in the same region of x_{Bj} and Q^2. R_2 is measured in bins of x_{Bj}, integrated over Q^2, and in bins of Q^2, integrated over x_{Bj}.

5 Data Correction

The residual background from photoproduction processes was determined using the PHOJET Monte Carlo (MC) generator [11] and was separately subtracted from the total number of events and the di-jet events as a function of Q^2 and x_{Bj}. This generator has been proven to give a good description of photoproduction background [6]. The correction for this background as well as the other corrections described below were obtained using MC events which were processed by the H1 detector simulation, reconstruction, and analysis chain. The largest subtraction of the photoproduction background occurs in the lowest x_{Bj} and Q^2 bins, where it amounts to 14% and 9% of the total event sample respectively, and to 3% and 1% of the di-jet sample. It is below 5% in the total sample and negligible in the di-jet sample in all other bins. For the di-jet rate, the correction is only significant in the lowest x_{Bj} and Q^2 bins where it increases the rate by $\approx 10\%$.

Radiation of photons from the incoming or outgoing positron leads to values of x_{Bj}, Q^2, and y, as determined from the scattered positron, which differ from the true kinematics of the photon-proton interaction.[5] These effects are different for the total and the di-jet sample. They were corrected using the DJANGO MC generator [12]. The correction factor on the di-jet rate was found to be 1.08, independent of x_{Bj} and Q^2.

[4] Several initial cone centres may result in the same candidate jet.

[5] In the outgoing positron case, this only applies if the angle between the radiated photon and the outgoing positron is large.

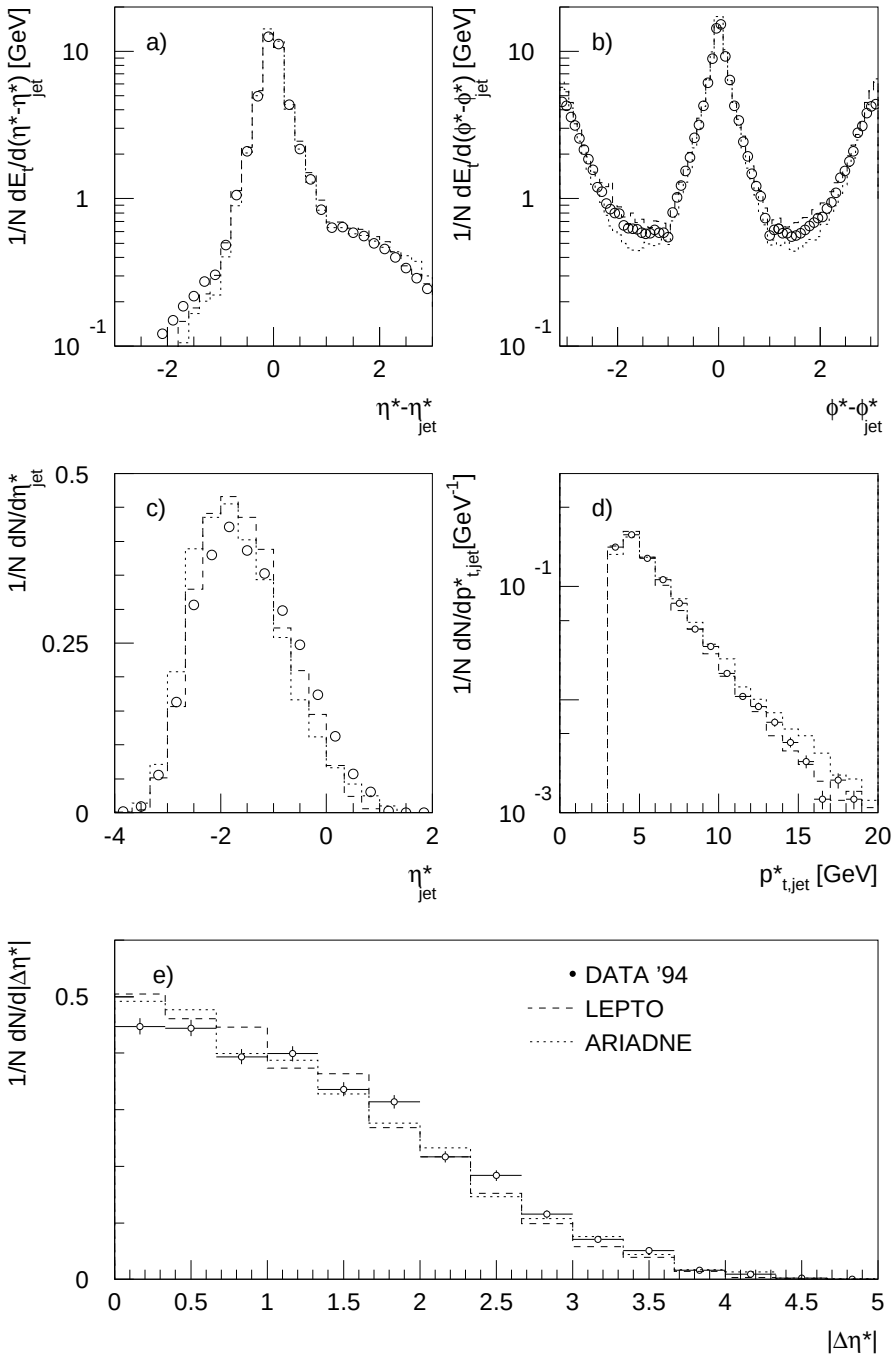

Figure 1: *Transverse energy flow with respect to the jet axis, a) versus $\eta^* - \eta^*_{\rm jet}$ in a slice defined by $|\phi^* - \phi^*_{\rm jet}| < 1$, b) versus $\phi^* - \phi^*_{\rm jet}$ in a slice defined by $|\eta^* - \eta^*_{\rm jet}| < 1$. In the Figs. c) and d) the η^* and p^*_t spectra of the jets are shown. In Fig. e) the $|\Delta\eta^*|$ distribution is displayed. Points denote data, the histograms indicate the distributions obtained from LEPTO (dashed) and ARIADNE (dotted). The curves are normalized to the number N of entries; there are two entries per di-jet event in Figs. a)–d) and one in Fig. e). For Fig. d), $p^*_{t,\rm min}$ (Eqn. 2) was lowered to 3.5 GeV and for Fig. e), the cut on $|\Delta\eta^*|$ (Eqn. 3) was omitted.*

The correction of the di-jet rate for detector acceptance and efficiencies was performed with two MC models, LEPTO [13] and ARIADNE [14], which will be discussed in section 7. They were used with two sets of parton density parameterizations, MRS-H [15] and GRV-94 HO [16] as implemented in PDFLIB [17]. The average prediction of these models was used to obtain bin-wise correction factors $c = \mathrm{R}_2^{\mathrm{MC,hadrons}}/\mathrm{R}_2^{\mathrm{MC,recon.}}$ for the di-jet rate R_2. This procedure is justified since the observables of the jet events, which are sensitive to detector effects, are well described by the Monte Carlo simulations. Critical observables in this sense are the energy flow within and around the jets, the η^* and p_t^* distribution of the two jets and the pseudo-rapidity difference $|\Delta\eta^*|$ between them.

Fig. 1 shows a comparison of the experimental distributions with the two MC models. Only the curves obtained with the MRS-H parton density are shown, the curves with GRV-94 HO are very similar. There is good agreement between data and simulated events except for the η^* distribution of the jets. On top of the bin-wise correction, which ignores this small discrepancy, an additional correction for this effect was applied [8]. It takes into account the fact that on average the η^* of the jets for data is higher than for MC which leads to an overestimation of the correction factors c, as the jet reconstruction efficiency depends on η^*. This correction reduces R_2 by 10% in the lowest and by 1% in the uppermost bins of Q^2 and x_{Bj}. The combined correction factors vary between 1.0 for low x_{Bj} and Q^2 values and 1.2 for high values.

6 Systematic Errors

Several sources of systematic uncertainties were investigated. A change in the hadronic energy scale of the LAr calorimeter by its estimated precision of $\pm 4\%$ results in a global change of the di-jet rates by $^{+9\%}_{-7\%}$. The correction for radiative effects has a global uncertainty of $\pm 3\%$ based on Monte Carlo statistics. These two errors were added in quadrature to give an overall systematic error of $^{+10\%}_{-8\%}$.

Changing the energy scale of the positron measurement in the BEMC within its $\pm 1\%$ uncertainty results in a change of R_2 by $\pm 2\%$ in all Q^2 bins. In the x_{Bj} bins, the change varies between $\pm 1\%$ for the lowest and $\pm 9\%$ for the highest bin. The systematic errors on the corrections for acceptance and efficiency were obtained by using the maximal variation of the correction factor for any particular model compared to the mean in each bin. They are of the order of 10%. The additional corrections for the difference in the mean values of η^* between experiment and simulation have a systematic error of the order of 2%. These errors were added in quadrature to give a bin by bin systematic error. It varies between 5% and 19%.

7 QCD Calculation of Di-jet Rates

Scattering processes involving the production of high p_T partons (hard scattering processes) are expected to be well described by perturbative QCD. In this analysis hard collisions are selected by requiring two jets with transverse momentum above 5 GeV. We consider three different QCD inspired models labeled DIR (direct), DIR+RES (direct +

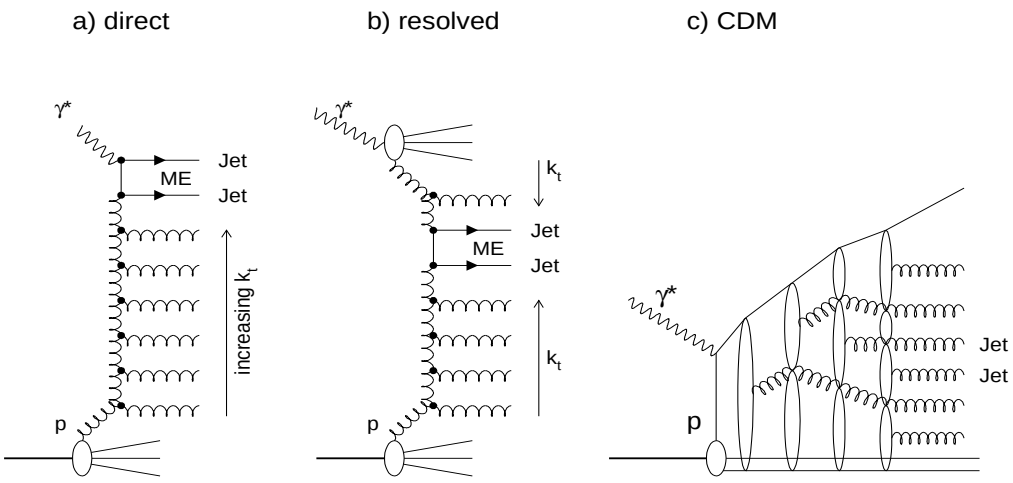

Figure 2: *Generic diagrams of initial state parton emission in ep scattering (a,b). In the direct process (a) the hardest emission given by the QCD matrix element occurs at the top of the ladder. Emissions down the ladder are ordered with decreasing transverse momenta k_t. In the resolved process (b) the hardest emission given by the QCD matrix element may occur anywhere in the ladder with increasingly soft emissions along the ladder towards the proton and the photon. In the colour dipole model (c) gluon emissions are not ordered in transverse momentum k_t.*

resolved), CDM (colour dipole model), and NLO QCD calculations at the parton level for comparison with experimental data. We briefly describe their most important features.

DIR: The LO QCD matrix elements (BGF and QCDC) are convoluted with the parton densities in the proton. Only direct interactions of the photon are considered as indicated in Fig. 2a. For this model we have used the LEPTO [13] and RAPGAP [18] MC programs. The latter has been used without generating diffractive (rapidity gap) processes. RAPGAP and LEPTO give results consistent with each other to better than 10%.

DIR+RES: In addition to the direct contribution discussed above, a contribution from quarks and gluons inside the photon is considered, as shown in Fig. 2b. This resolved photon contribution is assumed to set in only for scales of the hard subprocess $\gtrsim Q^2$. For the virtual photon parton densities the SaS-1D parameterization [19] was used. For this set of parton densities, the scale of the onset of the anomalous contribution in the virtual photon $P_0^2 = \max(Q_0^2, Q^2)$ was chosen, where $Q_0^2 = 0.36$ GeV^2 is the starting point of the Q^2 evolution[6]. The LO resolved photon contribution is implemented in the RAPGAP program. The contribution from longitudinal virtual photons is neglected.

[6] this corresponds to the SaSgam parameter IP2=2

In both the DIR and DIR+RES models we have used for the renormalization and factorization scale $\mu^2 = Q^2 + p_t^2$ as it provides a smooth transition between the DIS and photoproduction regimes. Additional emissions in the initial and final state are generated by parton showers [20] in the leading log DGLAP [21] approximation. In this approximation the radiated partons in the initial state are strongly ordered in transverse momentum k_t[7], with the hardest emission in the ladder occurring next to the hard matrix element (Figs. 2a and 2b).

CDM: In the colour dipole model [22], as implemented in the MC generator ARIADNE [14], gluon emission originates from a colour dipole stretched between the scattered quark and the proton remnant. Each emission of a gluon leads to two dipoles which may radiate further, generating a cascade of independently radiating dipoles (Fig. 2c). These gluons are not ordered in k_t. A similar feature is found in the BFKL [23] evolution scheme.

The colour charge of the proton remnant (a di-quark in the simplest case) is assumed not to be point-like, leading to a phenomenological suppression of gluon radiation [14] in the direction of the remnant. This suppression occurs for hard gluons with wavelengths smaller than the size of the remnant. In addition, the colour charge of the scattered quark is taken to be extended, depending on the virtuality Q^2 of the photon (photon size suppression). This in turn leads to a suppression of radiation in the direction of the scattered quark [14, 24].

The QCDC component of the di-jet rate depends in the CDM model on the size of the colour charge while for the DIR model it depends on the parton densities of the proton. At low x_{Bj} this results in a considerably enhanced di-jet rate for CDM compared to DIR [25]. The photon-gluon fusion process, which is not naturally described by the CDM, is treated similarly as in the DIR approach discussed above.

In the DIR, DIR+RES, and CDM models, hadronization was performed with the Lund string fragmentation scheme as implemented in JETSET [26].

NLO: Finally, we consider two calculations in next to leading order (NLO) in the strong coupling constant α_s as implemented in the Monte Carlo integration programs DISENT [27] and JETVIP [28]. These programs provide cross sections for partons rather than a full hadronic final state. DISENT takes the soft and collinear divergencies arising in any NLO QCD calculation into account by using the subtraction method while JETVIP relies on the phase space slicing method. Both DISENT and JETVIP calculate NLO cross sections assuming a direct interacting photon. In addition, JETVIP provides a consistent calculation in NLO of direct *and* resolved interacting photons using parameterizations of the virtual photon structure functions. For the latter, the SaS-1D parameterization [19] (transformed to $\overline{MS}$) was used. For both the DISENT and JETVIP calculations the factorization and renormalization scales were chosen to be $\mu^2 = Q^2 + 50$ GeV^2, where 50 GeV^2 represents a good estimate of the average transverse momentum squared of the jets in the hadronic cms for the selection described before.

[7] k_t is the transverse momentum relative to the proton and photon axis in the photon-proton cms.

For comparing the corrected di-jet rate with models and parton level calculations, we have used the CTEQ4M parameterization [29] of parton densities inside the proton with the corresponding $\Lambda^{(5)}_{\overline{MS}}$ of 202 MeV (different parton density parameterizations were used in the models used to correct for detector effects, c.f. section 5). The DIR, RES, and CDM models implement the one loop expression for the calculation of α_s and in the DISENT and JETVIP programs the two loop expression was used.

8 Results and Discussion

The di-jet rate R_2 is shown in Figs. 3a and 3b as a function of Q^2 and x_{Bj} respectively. The data have been corrected for detector effects to the hadron level. The results correspond to the phase space region defined by Eqs. 1–3. The data show a jet rate rising with Q^2 and flat in x_{Bj} except for the highest x_{Bj}-value.

For reasons to be explained later, two further scenarios have been investigated, where in addition to our basic requirement of $p_t^* > 5$ GeV for each jet (symmetric scenario), we demand either at least 7 GeV for the jet with the highest p_t^* (asymmetric scenario) or at least 13 GeV for the sum of the absolute values of the jet transverse momenta (sum scenario). The results for R_2 for the asymmetric scenario are given in Figs. 3c,d and for the sum scenario in Figs. 3e,f. Table 1 in the appendix summarizes the di-jet rates for the three different scenarios.

8.1 Comparison of data with LO QCD models

The results for the three different selections of jet phase space are compared to predictions from MC models based on perturbative QCD (see previous section). The LO DIR model fails to describe the data as demonstrated in Figs. 3a to 3f with RAPGAP. In particular in the region of small Q^2 and x_{Bj} the DIR model underestimates the data by a factor 2–3.

Choosing $\mu^2 = Q^2$ for the hard scale does not change the results considerably. Using different parton density parameterizations (CTEQ4L, CTEQ4A4, CTEQ4HJ, MRSR1, and MRSR2) leads to variations in R_2 of up to 10% in the lowest and the highest Q^2 and x_{Bj} bins when compared to CTEQ4M, our default. The world average value of $\alpha_s(M_Z^2) = 0.118$ corresponds to $\Lambda^{(5)}_{\overline{MS}} = 209^{+39}_{-33}$ MeV [30], very close to the fit value of 202 MeV for CTEQ4M. With the CTEQ4M parton densities but with $\Lambda^{(5)}_{\overline{MS}} = 250$ MeV (an increase of about one standard deviation), R_2 increases by less than 10% in the lowest Q^2 and x_{Bj} bins.

We conclude that a LO matrix element calculation assuming only direct interactions of the virtual photon in combination with DGLAP parton showers as an approximation to higher order effects is not able to account for the observed di-jet rates.

Adding a significant contribution to the di-jet cross section from resolving the structure of the virtual photon, as predicted by the DIR+RES model as implemented in RAPGAP, gives a good description of the data. It should be noted, however, that considerable freedom exists in tuning the model to data, in particular by varying the choice of the hard scale, and the parton densities in the virtual photon.

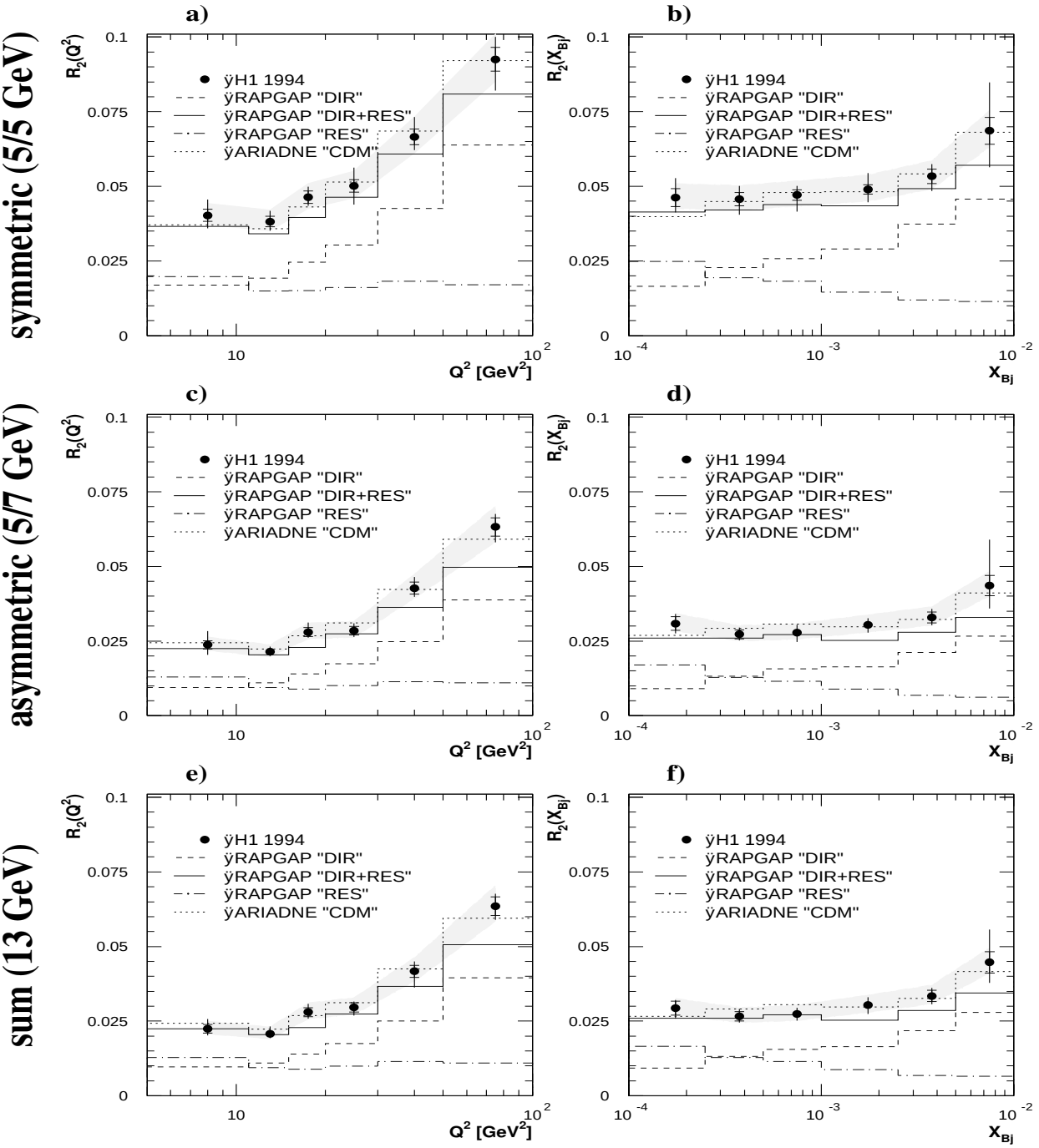

Figure 3: *Di-jet rate* R_2 *as a function of* Q^2 *(a,c,e), integrated over* x_{Bj}*, and as a function of* x_{Bj} *(b,d,f), integrated over* Q^2 *for the symmetric (a,b), asymmetric (c,d), and sum (e,f) cut scenario on the* p_t^* *of the two jets. The data are corrected to the hadron level. The inner bars give the statistical errors, the full error bars include the bin by bin systematic errors. The grey band shows the overall systematic uncertainty due to the hadronic energy scale of the calorimeter and the uncertainty of the radiative correction. Also indicated are the predictions from MC models. Their statistical errors are smaller than the statistical errors of the data.*

The CDM model, as implemented in ARIADNE, is also able to describe the di-jet rate well, both in absolute value and in the Q^2 and x_{Bj} dependence. We used a parameter setting which had been tuned to give a good description of transverse energy flows and particle spectra [31]. Here too, it should be remarked that by varying the parameters for the proton and photon size suppression (see section 2) within sensible limits[8], the predictions of this model can be changed by up to 40% in the lowest bin and about 20% in the highest bin in Q^2 and x_{Bj}.

8.2 Comparison of data with NLO QCD calculations

We now investigate whether a NLO QCD calculation is able to describe the data. For this purpose we have used results from the programs DISENT and JETVIP [28]. For the calculation of R_2 for the direct or point-like coupling of the photon to the partons in the proton, the two programs agree to better than 5%. As mentioned in section 7, JETVIP can also calculate the direct and resolved photon contribution in NLO. Both programs provide parton level cross sections rather than a full hadronic final state. However, the DIR and CDM models suggest that the hadronization effects are small for jet transverse momenta above 5 GeV. The di-jet rate at the parton level was found to be for LEPTO (ARIADNE) typically 9% (20%) and not more than 12% (25%) higher than the rate at the hadron level.

Figs. 4a,b show the hadron level di-jet rate R_2 versus Q^2 and x_{Bj} for the asymmetric scenario, and in Figs. 4c,d for the sum scenario, compared to the NLO QCD calculation of the direct contribution (labeled DIR in the figures) by JETVIP and DISENT. Good agreement is observed between data and the direct NLO QCD calculation, except for the lowest Q^2 and x_{Bj} bin.

The sensitivity to variations of the parton density parameterizations is similar to the LO DIR case discussed above. Varying the factorization and renormalization scale μ^2 by factors of 4 results in cross section variations of less than 20%. Choosing $\mu^2 = Q^2$ as the scale enhances the cross section in the lowest x_{Bj} and Q^2 bins by up to 30%, improving the agreement with data. At the same time this introduces however a large sensitivity to scale variations (up to 50% and 65% in the lowest Q^2 and x_{Bj} bins). This indicates, as one might expect, that Q^2 is not the proper scale to use in a kinematic domain where $Q^2 \ll p_t^2$.

The agreement with data at low x_{Bj} and Q^2 is improved when contributions from resolving the virtual photon structure are included in NLO (labeled DIR-PSP+RES in the figure). In order to avoid double counting in the full NLO QCD calculation it is necessary to subtract the contribution from the virtual photon splitting into $q\bar{q}$, where one of the quarks subsequently interacts with a parton from the proton to produce two high p_t jets, since this contribution is part of the parameterization of the virtual photon structure function [19]. We refer to this perturbatively calculated contribution from photon splitting as defined in [28] as PSP and the contribution from resolving the photon structure as RES.

Two interesting observations can be made. First, at large Q^2 the difference between the NLO direct part (DIR) and the full calculation (DIR-PSP+RES) is found to be rather

[8] PARA(10) and PARA(15), default 1.0 [14]; we used 1.5 and 0.5 respectively and varied them independently between 0.5 and 1.5.

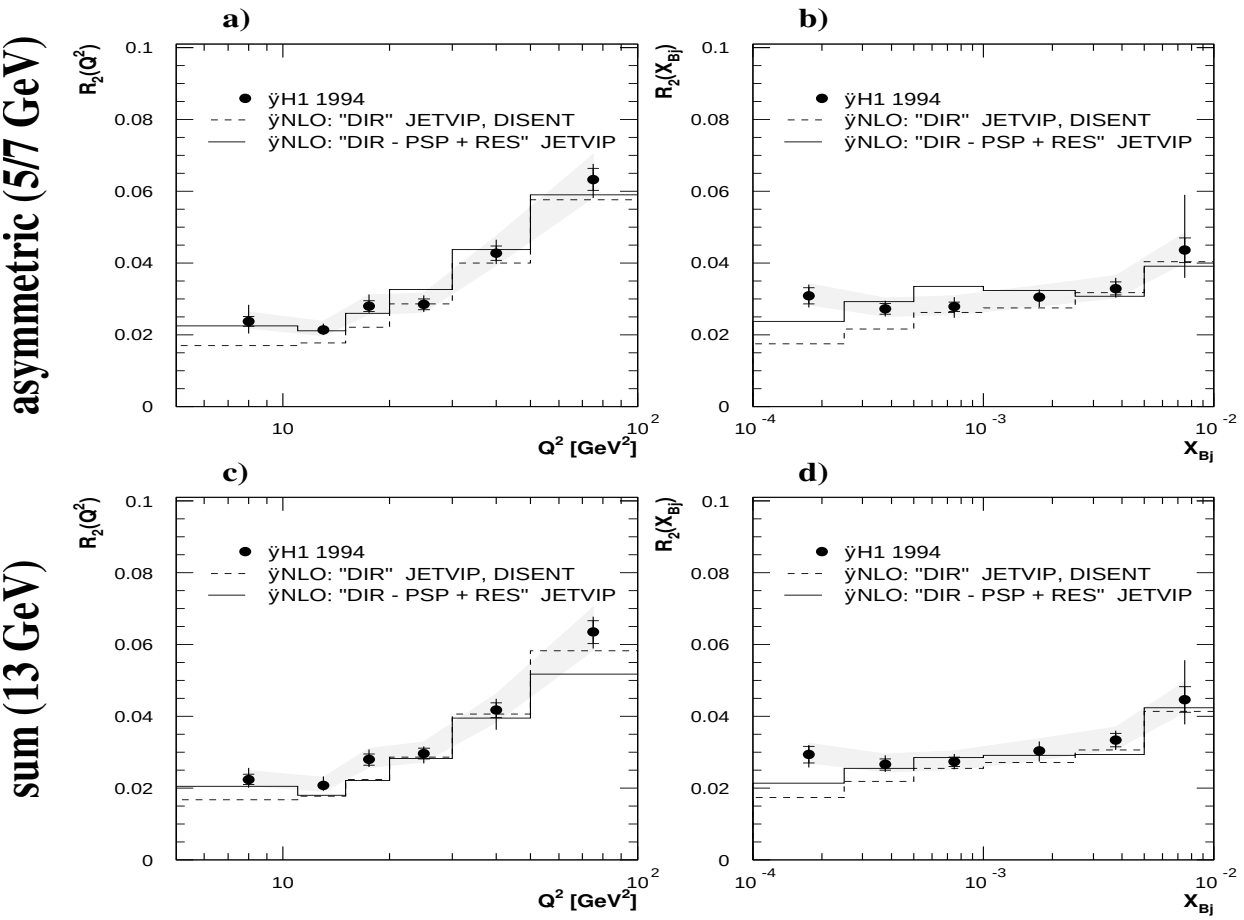

Figure 4: *Di-jet rate* R_2 *as a function of* Q^2 *(a,c), integrated over* x_{Bj}*, and as a function of* x_{Bj} *(b,d), integrated over* Q^2*. The data (corrected to the hadron level) for the asymmetric (a,b) and the sum scenario (c,d) are compared to different NLO calculations (at the parton level). The data are the same as those shown in Figs. 3c to 3f. The statistical errors of the NLO calculations are smaller than the statistical errors of the data.*

small, which implies that the NLO resolved part (RES) is saturated by the contribution from virtual photon splitting (PSP). Second, the full NLO calculation is close to the LO RAPGAP DIR+RES prediction shown as the full line in Figs. 3c to 3f. This suggests, together with the first observation, that the large resolved contribution needed in LO to describe the data for the larger Q^2 bins is included in the NLO DIR cross section.

It should be noted that in NLO the RES contribution depends less on the choice of the hard scale and the parton densities in the virtual photon than in LO. This is due to the subtraction procedure and because it is a NLO calculation [28]. Of course the uncertainty due to the rather poorly known parton density of the virtual photon remains.

A comparison of the data on R_2 and the NLO QCD calculation for the symmetric scenario is not shown, because the calculation for this case is not reliable although the measurement is valid and infrared safe. The calculations from both DISENT and JETVIP underestimate the data and give different predictions. This can be understood as a feature of any fixed order calculation which gives large negative cross sections in the phase space region where both jets have almost identical transverse momenta. The problem in the prediction of di-jet rates for symmetric cuts on the jet transverse momenta has been noted in the framework of the phase space slicing method [32] and discussed in detail for this and the subtraction method in [33]. A correct treatment of this phase space region would need a resummation to all orders [33, 34].

8.3 Event topology

The conclusions of the underlying picture derived above can be checked by a study of the event topology. In the DIR+RES model the hardest emission leading to the observed jets may occur anywhere in the ladder, as depicted in Fig. 2b. In this case, additional hadronic activity is expected from the virtual photon "remnant" and additional parton emission from the top part of the ladder.

This activity is expected in the direction of the virtual photon which corresponds to the backward region of the detector. Similar hadronic activity in the backward region can also be expected from the CDM model due to the absence of k_t ordering between the photon and the proton vertex (see section 2). Both models predict a Q^2 dependence of this effect which increases as Q^2 approaches zero.

We define an observable which is sensitive to additional energy flow in the photon direction:

$$x_\gamma^{\mathrm{obs}} = \frac{\sum_{\mathrm{jets}} (E - p_z)}{\sum_{\mathrm{had.\ final\ state}} (E - p_z)} \tag{4}$$

In the limit $Q^2 \to 0$ and in LO this corresponds to the fractional momentum of the parton from the photon entering the hard subprocess and giving rise to the observed jet system. In this picture $1 - x_\gamma^{\mathrm{obs}}$ corresponds to the fractional energy of the photon remnant.

Fig. 5a shows the uncorrected distribution of x_γ^{obs} for data in three different ranges of Q^2. The MC events which were used for comparison in Fig. 5 have been subject to a detailed simulation of the H1 detector. In the data an increase at low x_γ^{obs} is noticed as

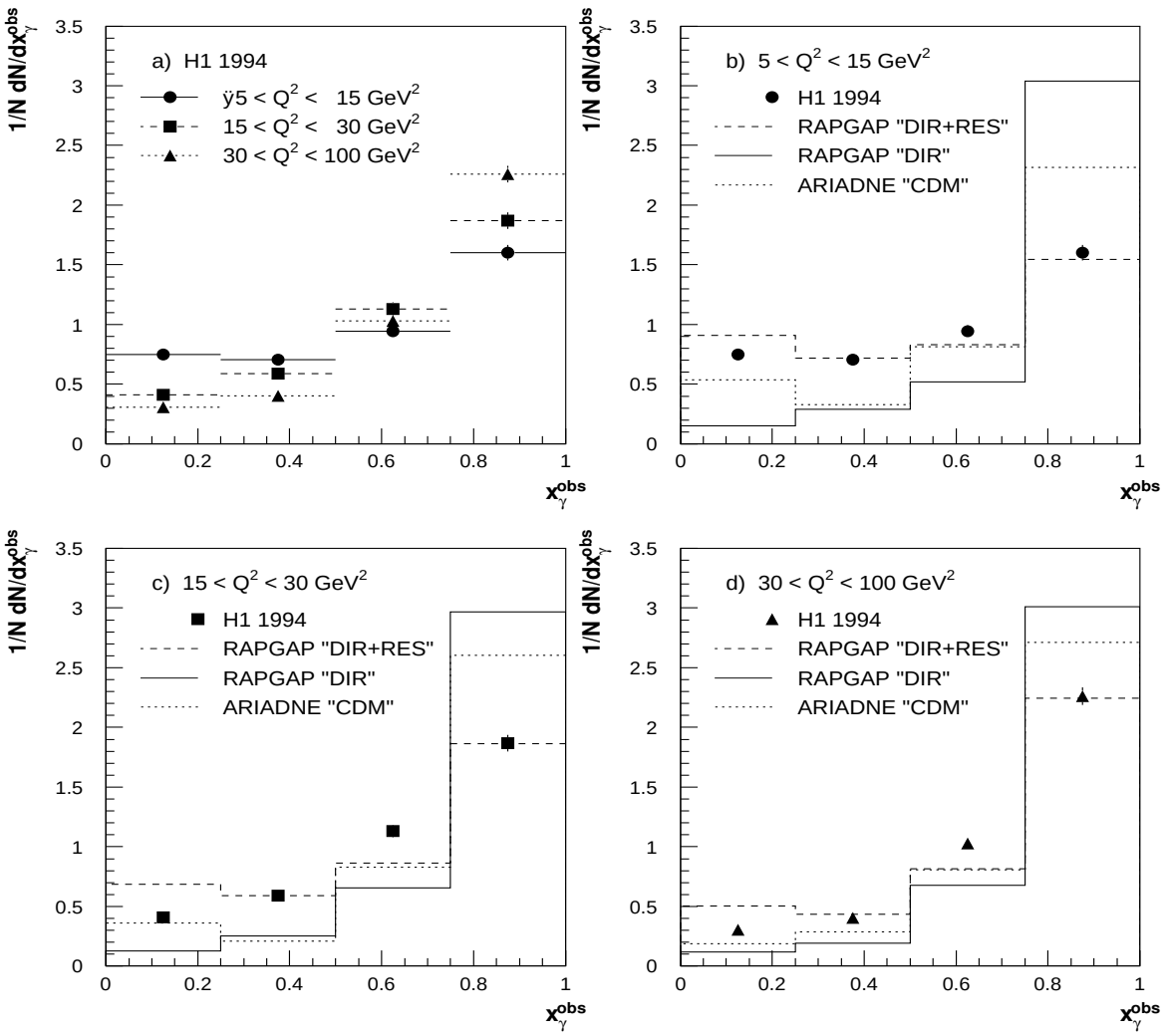

Figure 5: *Uncorrected distribution of $x_\gamma^{\rm obs}$ in three different Q^2 bins (a). In b) to d) the data are compared for each bin in Q^2 to the DIR model and the DIR+RES model as given by RAPGAP, and the CDM model as implemented by ARIADNE. The figures are normalized to the number N of di-jet events. The error bars indicate the statistical error only.*

Q^2 decreases. No such effect is seen for the DIR model as represented by RAPGAP (full line in Figs. 5b to 5d). The DIR+RES model of RAPGAP is able to give a reasonable description of both shape and Q^2 dependence (dashed line in Figs. 5b to 5d). The CDM model shows a similar Q^2 dependence but fails to describe the shape of the distribution (dotted line in Figs. 5b to 5d).

9 Conclusions

Di-jet event rates have been measured in deep-inelastic scattering at small x_{Bj} ($10^{-4} \lesssim x_{Bj} \lesssim 10^{-2}$) and moderate Q^2 ($5 \lesssim Q^2 \lesssim 100$ GeV^2). Three different scenarios of cuts on the transverse momenta of the jets have been investigated: the basic symmetric requirement ($p^*_{t,\mathrm{min}} \geq 5\,\mathrm{GeV}$ for both jets), and additionally the asymmetric ($p^*_{t,\mathrm{min}} \geq 5$ and $7\,\mathrm{GeV}$) and sum p^*_t ($\geq 13\,\mathrm{GeV}$) requirements. The analysis was performed in the hadronic centre of mass frame. The data have been corrected for detector and QED radiative effects. This analysis probes a region in jet phase space of small x_{Bj} and jet transverse momenta squared of similar size or larger than the photon virtuality ($p^2_t/Q^2 \gtrsim 1$).

Assuming a direct or point-like photon, leading order matrix element calculations in combination with parton showers as an approximation of higher order effects fail completely to describe the data.

Adding to the leading order model additional contributions from resolving the partons inside the virtual photon (RAPGAP) appear to give an effective description of higher order effects leading to good agreement with the data for all three scenarios. A similarly good agreement with the di-jet event rates is observed for the colour dipole model (ARIADNE) with its features of gluon emission.

Next-to-leading order calculations in α_s assuming a point-like virtual photon provide a good description of the data for the scenarios with the asymmetric and the sum p^*_t cut, except for the lowest bin in Q^2 and x_{Bj}. This is improved by a NLO calculation which also considers contributions from resolving virtual photon structure.

Acknowledgements

We are grateful to the HERA machine group whose outstanding efforts have made and continue to make this experiment possible. We thank the engineers and technicians for their work in constructing and now maintaining the H1 detector, our funding agencies for financial support, the DESY technical staff for continual assistance, and the DESY directorate for the hospitality which they extend to the non-DESY members of the collaboration. We gratefully acknowledge fruitful discussions with S. Frixione, G. Kramer, L. Lönnblad, B. Pötter, and J. Rathsman.

Appendix

	symmetric (5/5 GeV)			asymmetric (5/7 GeV)			sum (13 GeV)		
Q^2 [GeV^2]	R_2	σ_{stat}	σ_{syst}	R_2	σ_{stat}	σ_{syst}	R_2	σ_{stat}	σ_{syst}
5 – 11	0.040	± 0.002	$^{+0.005}_{-0.004}$	0.024	± 0.001	$^{+0.004}_{-0.003}$	0.022	± 0.001	$^{+0.003}_{-0.002}$
11 – 15	0.038	± 0.002	$^{+0.003}_{-0.002}$	0.021	± 0.001	$^{+0.001}_{-0.001}$	0.021	± 0.001	$^{+0.002}_{-0.001}$
15 – 20	0.046	± 0.002	$^{+0.003}_{-0.002}$	0.028	± 0.002	$^{+0.003}_{-0.001}$	0.028	± 0.002	$^{+0.002}_{-0.002}$
20 – 30	0.050	± 0.002	$^{+0.006}_{-0.006}$	0.028	± 0.001	$^{+0.002}_{-0.002}$	0.030	± 0.002	$^{+0.001}_{-0.002}$
30 – 50	0.067	± 0.003	$^{+0.006}_{-0.004}$	0.043	± 0.002	$^{+0.003}_{-0.002}$	0.042	± 0.002	$^{+0.003}_{-0.005}$
50 – 100	0.093	± 0.004	$^{+0.006}_{-0.010}$	0.063	± 0.003	$^{+0.003}_{-0.004}$	0.063	± 0.003	$^{+0.003}_{-0.003}$

	symmetric (5/5 GeV)			asymmetric (5/7 GeV)			sum (13 GeV)		
x_{Bj}	R_2	σ_{stat}	σ_{syst}	R_2	σ_{stat}	σ_{syst}	R_2	σ_{stat}	σ_{syst}
$10^{-4} - 2.5 \cdot 10^{-4}$	0.046	± 0.003	$^{+0.006}_{-0.004}$	0.031	± 0.002	$^{+0.002}_{-0.002}$	0.029	± 0.002	$^{+0.001}_{-0.003}$
$2.5 \cdot 10^{-4} - 5.0 \cdot 10^{-4}$	0.046	± 0.002	$^{+0.004}_{-0.005}$	0.027	± 0.002	$^{+0.002}_{-0.001}$	0.027	± 0.002	$^{+0.002}_{-0.001}$
$5.0 \cdot 10^{-4} - 10^{-3}$	0.047	± 0.002	$^{+0.003}_{-0.005}$	0.028	± 0.001	$^{+0.002}_{-0.003}$	0.027	± 0.001	$^{+0.002}_{-0.002}$
$10^{-3} - 2.5 \cdot 10^{-3}$	0.049	± 0.002	$^{+0.005}_{-0.004}$	0.030	± 0.001	$^{+0.002}_{-0.002}$	0.030	± 0.001	$^{+0.002}_{-0.003}$
$2.5 \cdot 10^{-3} - 5.0 \cdot 10^{-3}$	0.053	± 0.002	$^{+0.003}_{-0.004}$	0.033	± 0.002	$^{+0.002}_{-0.002}$	0.033	± 0.002	$^{+0.002}_{-0.002}$
$5.0 \cdot 10^{-3} - 10^{-2}$	0.069	± 0.005	$^{+0.016}_{-0.011}$	0.044	± 0.003	$^{+0.015}_{-0.007}$	0.045	± 0.004	$^{+0.010}_{-0.006}$

Table 1: *Di-jet rate in bins of Q^2 and x_{Bj}, and statistical and systematic errors for the symmetric, the asymmetric, and the sum cut scenario on the p_t^* of the two jets. The overall systematic error of $^{+10\%}_{-8\%}$ for the symmetric scenario and $^{+11\%}_{-8\%}$ for the asymmetric and sum scenario, arising from the uncertainty of the hadronic energy scale of the calorimeter and the uncertainty of the radiative QED corrections, is not included.*

References

[1] H1 Collaboration, I. Abt et al.,Z. Phys. C61 (1994) 59;
ZEUS Collaboration, M. Derrick et al., Z. Phys. C67 (1995) 81.

[2] H1 Collaboration, C. Adloff et al., Phys. Lett. B415 (1997) 418.

[3] H1 Collaboration, I. Abt et al., Nucl. Instr. and Meth. A386 (1997) 310 and 348.

[4] H1 Calorimeter Group, B. Andrieu et al., Nucl. Instr. and Meth. A336 (1993) 460.

[5] H1 BEMC Group, J. Ban et al., Nucl. Instr. and Meth. A372 (1996) 399.

[6] H1 Collaboration, S. Aid et al., Nucl. Phys. B470 (1996) 3.

[7] H1 Calorimeter Group, B. Andrieu et al., Nucl. Instr. and Meth. A336 (1993) 499.

[8] J. Spiekermann, Ph.D. Thesis, University of Dortmund (1997).

[9] M.H. Seymour, Z. Phys. C62 (1994), 127.

[10] M.H. Seymour, Nucl. Phys. B421 (1994) 545.

[11] R. Engel, Z. Phys. C 66 (1995) 203;
R. Engel and J. Ranft, Phys. Rev. D54 (1996) 4244.

[12] K. Charchula, G. A. Schuler, and H. Spiesberger, Comput. Phys. Commun. 81 (1994) 381.
We used the program version 6.2.

[13] G. Ingelman, in Proc. Workshop on Physics at HERA, Hamburg, October 1991, eds. W. Buchmüller and G. Ingelman, vol. 3 (1992) 1366;
G. Ingelman, A. Edin, J. Rathsman, Comput. Phys. Comm. 101 (1997) 108.
We used the program versions 6.4 and 6.5.

[14] L. Lönnblad, Comput. Phys. Comm. 71 (1992) 15;
L. Lönnblad, Z. Phys. C65 (1995) 285.
We used the program version 4.08.

[15] A.D. Martin, W.J. Stirling, and R.G. Roberts, in Proc. Workshop on Quantum Field Theory and Theoretical Aspects of High Energy Physics, Bad Frankenhausen, Germany, 1993, eds. B. Geyer and E.M. Ilgenfritz, (1993) 11.

[16] M. Glück, E. Reya, and A. Vogt, Z. Phys. C67 (1995) 433.

[17] H. Plothow-Besch, Int. J. Mod. Phys. A10 (1995) 2901.
We used the library version 7.09.

[18] H. Jung, Comput. Phys. Commun. 86 (1995) 147.
We used the program version 2.06.

[19] G. A. Schuler and T. Sjöstrand, Z. Phys. C68 (1995) 607, Phys. Lett. B376 (1996) 193.

[20] M. Bengtsson and T. Sjöstrand, Z. Phys. C37 (1988) 465.

[21] V. N. Gribov and L. N. Lipatov, Sov. J. Nucl. Phys. 15 (1972) 438;
G. Altarelli and G. Parisi, Nucl. Phys. B126 (1977) 298;
Yu. L. Dokshitzer, Sov. Phys. JETP 46 (1977) 641.

[22] G. Gustafson, Phys. Lett. B175 (1986) 453;
G. Gustafson and U. Petterson, Nucl. Phys. B306 (1988) 746;
B. Andersson, G. Gustafson, L. Lönnblad, and U. Petterson, Z. Phys. C43 (1989) 625.

[23] E. A. Kuraev, L. N. Lipatov, and V. S. Fadin, Sov. Phys. JETP 45 (1977) 199;
Ya. Ya. Balitsky and L. N. Lipatov, Sov. J. Nucl. Phys. 28 (1978) 822;
J. Bartels and H. Lotter, Phys. Lett. B309 (1993) 400.

[24] L. Lönnblad, M. H. Seymour, et al., Proc. Physics at LEP 2 Workshop, eds. G. Altarelli, T. Sjöstrand, and F. Zwirner, CERN/96-01, Vol. 2, (1996) 187.

[25] J. Rathsman, Phys. Lett. B393 (1997) 181.

[26] T. Sjöstrand, Comp. Phys. Comm. 82 (1994) 74;
T. Sjöstrand, Pythia 5.7 and Jetset 7.4 physics and manual, CERN-TH 7112/93, Dec. 1993 (revised Aug. 1994).

[27] S. Catani and M. H. Seymour, Acta Phys. Polon. B28 (1997) 863.

[28] B. Pötter, Report DESY 98–071, [hep-ph/9806437];
G. Kramer and B. Pötter, Report DESY 98–046, [hep-ph/9804352].
The numerical results were provided for us by B. Pötter.

[29] H. L. Lai et al., Phys. Rev. D55 (1997) 1280.

[30] R.M. Barnett et al., Phys. Rev. D54 (1996) 1.

[31] N. Brook et al., in Proc. Workshop on Future Physics at HERA, Hamburg, September 1996, eds. G. Ingelman, A. De Roeck, R. Klanner, vol. 1 (1996) 613.

[32] M. Klasen and G. Kramer, Phys. Lett. B366 (1996) 385.

[33] S. Frixione and G. Ridolfi, Nucl. Phys. B507 (1997) 315.

[34] S. Catani and B. Webber, JHEP 10 (1997) 005.